IJCRT.ORG ISSN : 2320-2882

INTERNATIONAL JOURNAL OF CREATIVE RESEARCH THOUGHTS (IJCRT)

An International Open Access, Peer-reviewed, Refereed Journal

Study of Si-Sb-ZnO Composites' Electrochemical Properties

Dr. Gajendra Prasad Gadkar
Associate Professor
Department of Physics
College of Commerce, arts &science, Patliputra University, patna

Abstract

The Si-Sb-ZnO composites were ready by a substance decrease mechanical alloying technique and were utilized as anode materials for lithium-particle batteries. The addition of ZnO nanoparticles significantly enhanced the Si-Sb alloy's electrochemical performance. Particularly, the initial coulombic efficiency of 64.9 percent and the initial specific charge and discharge capacities of the Si-Sb-(ZnO)0.3 composite were 845.1 and 1301.5 mAh/g, respectively. The limit stayed at 690 mAh/g after 200 cycles, and the limit maintenance proportion was 81.6 %, which showed superb cycling dependability and rate ability of the composite materials.

Keywords: Lithium-ion batteries, Si-Sb-ZnO composite materials, Electrochemical properties

Background

Due to their high energy density, long cycle life, etc., lithium-ion batteries are promising energy storage systems for the rapidly expanding field of electric and hybrid vehicles [1–3]. Due to its low discharging potential, safety, and extremely high specific capacity of 4200 mAh/g, silicon (Si) is an ideal anode material for lithium-ion batteries. Be that as it may, poor electrical conductivity and the colossal volume change during lithium-particle addition/extraction processes are two basic impediments for Si-based anode materials [4, 5].

Si-based alloys have recently been developed to overcome these two drawbacks; The Si-M alloys (M = Mg [6, 7], Sn [8, 9], Ag [10, 11], Zn [12, 13], Fe [14, 15], and Ni [16, 17]) are able to reduce the volume expansion of the batteries, which in turn increases their cyclability. The immiscible Si-Sb alloy was created in our previous study, and it had a reversible capacity of 596.4 mAh/g and moderate electrochemical and cycling performance [18]. Despite this, the substantial volume expansion that occurs during charge/discharge processes causes the Si-based alloy particles to lose electrical contact with one another. As a result, Si-based anode materials' attractive research area has been enhancing cycling stability while maintaining high capacity.

Due to its high theoretical capacity, low cost, and abundance in nature, zinc oxide (ZnO) was one of the anode material options [19]. Notwithstanding, its unfortunate cyclability, brought about by volume development during the charge/release, influences the down to earth application [20-22]. In this work, ZnO was acquainted with the parallel Si-Sb materials by a compound decrease mechanical alloying strategy. ZnO has a high theoretical capacity of 978 mAh/g, which may increase the composite materials' specific capacity. ZnO was also able to effectively break up the Si-Sb alloy particles' agglomeration, preventing the volume

expansion-induced loss of electric contact between the electrode materials and the current collector. The dependence of the cyclic behavior of the electrodes was discussed as well as the electrochemical performance of composite Si-Sb-(ZnO)x anodes (x = 0, 0.1, 0.3, 0.5, 0.7, 0.9). The synthesized Si-Sb-(ZnO)0.3 composite anode material had an initial specific charge capacity of 870.3 mAh/g and a specific discharge capacity of 1301.5 mAh/g when the molar ratio of ZnO was 0.3. The Si-Sb-(ZnO)x composite anode materials' significantly improved cycling stability can be attributed to the fact that the addition of ZnO was able to effectively alleviate the agglomeration of the Si-Sb alloy particles.

Materials and Methods Synthesis All reagents were used without further purification and were of analytical quality. Chemical reduction-mechanical alloying was used to create the Si-Sb-(ZnO)x composite materials. In most cases, 0.1 mol of SbCl3, C6H5Na3O7, and Zn(NO3)2 in the following molar ratio: x (x = 0, 0.1, 0.3, 0.5, 0.7, 0.9) and a 0.2 mol NaBH4 solution in water with a pH above 12 were made, respectively. At room temperature, an excessive amount of NaBH4 was added dropwise to the SbCl3/Zn(NO3)2 solution with vigorous magnetic stirring. For the ball-milling procedure, the solutions were aged for 5 hours in a water bath at 80 °C. The precipitates were collected by centrifugation, washed with distilled water, and then mixed with 0.1 mol of Si nanopowders. After milling for 15 hours at 500 rpm in an argon atmosphere, the finished products were dried at 120 °C for 10 hours in a vacuum and stored in the glove box filled with argon.

Physical Characteristics A D8 Advance X-ray diffraction (XRD) instrument was used to examine the phases of the composite materials. Using a Hitachi Limited S-3400 N instrument, field-emission scanning electron microscopy (FE-SEM) was used to examine the particles' morphology and microstructure.

Electrochemical Characterizations

To evaluate their electrochemical properties, 70 wt.% of active materials, 15 wt.% of acetylene black and 15 wt.% of carboxyl methyl cellulose (CMC), and styrene butadiene rubber (SBR) were mixed to form slurry, which was then pressed onto a copper grid as electrodes and dried at 120 °C for 10 h under vacuum. The loading of active materials was about 1.2 mg cm^{-2} on the electrodes.

The electrochemical performances were measured using coin cells assembled in an argon-filled glove box; these cells contained metallic lithium foil as a counter electrode, 1 M $LiPF_6$ in ethylene carbonate (EC)-dimethyl carbonate (DMC) (1:1 v/v) as the electrolyte, Celgard 2400 membrane as a separator, and the synthesized composite alloy as a working electrode. The galvanostatic charge/discharge performance was assessed using a CT2001A battery tester from 0.1 to 2.0 V (vs. Li^+/Li) at a constant current density of 0.1 mA/cm^2 at room temperature unless noted. Cyclic voltammetry (CV) from 0 to 2.0 V (vs. Li/Li^+) at 0.01 mV/s and electrochemical impedance spectroscopy (EIS) in the frequency range 10^5 to 0.01 Hz and with an amplitude of 5 mV were performed using a Solartron 1470e electrochemical testing system.

Results and Discussion

Figure 1 shows the XRD patterns of Si-Sb-$(ZnO)_x$ composites obtained by chemical reduction-mechanical alloying method. The diffraction patterns of the composites consist of Si, Sb, and ZnO peaks, indicating that there is no intermetallic compound formed in the synthesis process. The characteristic peak intensities of Si and Sb are gradually increased with the ZnO content increased from 0 to 30 wt.%, and the peak intensities decreased when the ZnO content continued to increase. The results indicate that the Si-Sb-$(ZnO)_{0.3}$ composite possessed the best crystallinity. The back-scattered image of Si-Sb-$(ZnO)_{0.3}$ composite presented in Fig. 2 shows that Si, Sb, and ZnO are integrated without an apparent distinction in phases. According to the EDX analysis and the element mapping, the composite is consisted of Si (10.13 at.%), Sb (10.63 at.%), and Zn (2.91 at.%) in the scanning area, which are close to theoretical values (Table 1).

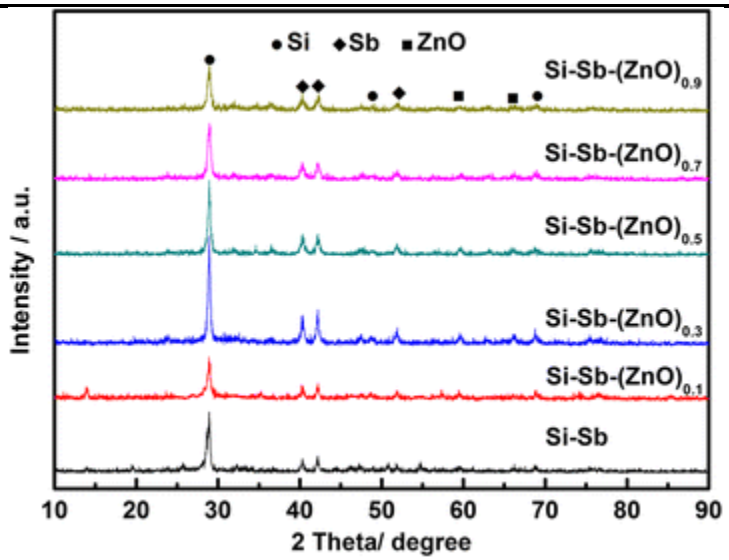

Fig. 1

XRD patterns of the Si-Sb-$(ZnO)_x$ composite materials

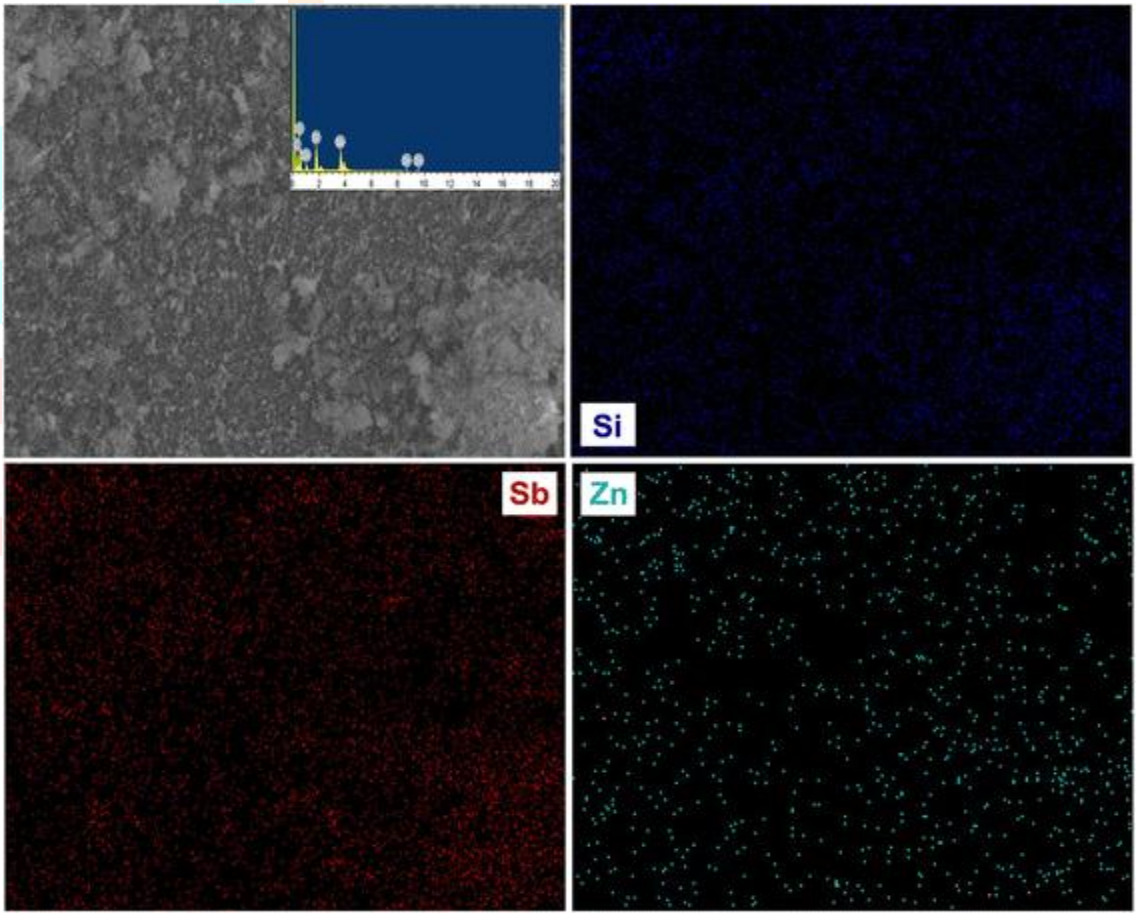

Fig. 2

SEM and the correlated elements mapping images for Si-Sb-$(ZnO)_{0.3}$anode material

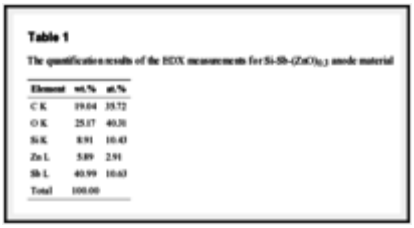

Table 1

The quantification results of the EDX measurements for Si-Sb-$(ZnO)_{0.3}$ anode material

Figure 3 shows the SEM images of Si-Sb-$(ZnO)_x$ ($x = 0$, 0.1, 0.3, 0.5, 0.7, 0.9) composite materials. As shown in Fig. 3a, the Si-Sb alloy particles are with irregular morphology and some of them are aggregated to form big particles. With the addition of ZnO, the distribution of the composite becomes uniform, indicating that ZnO plays a role in preventing the reunion, reducing the mechanical stress between the particles. The Si-Sb-$(ZnO)_x$ samples were composed of tiny particles which formed homogenous secondary particles; the particle size of the nano-composite materials was about 100 nm.

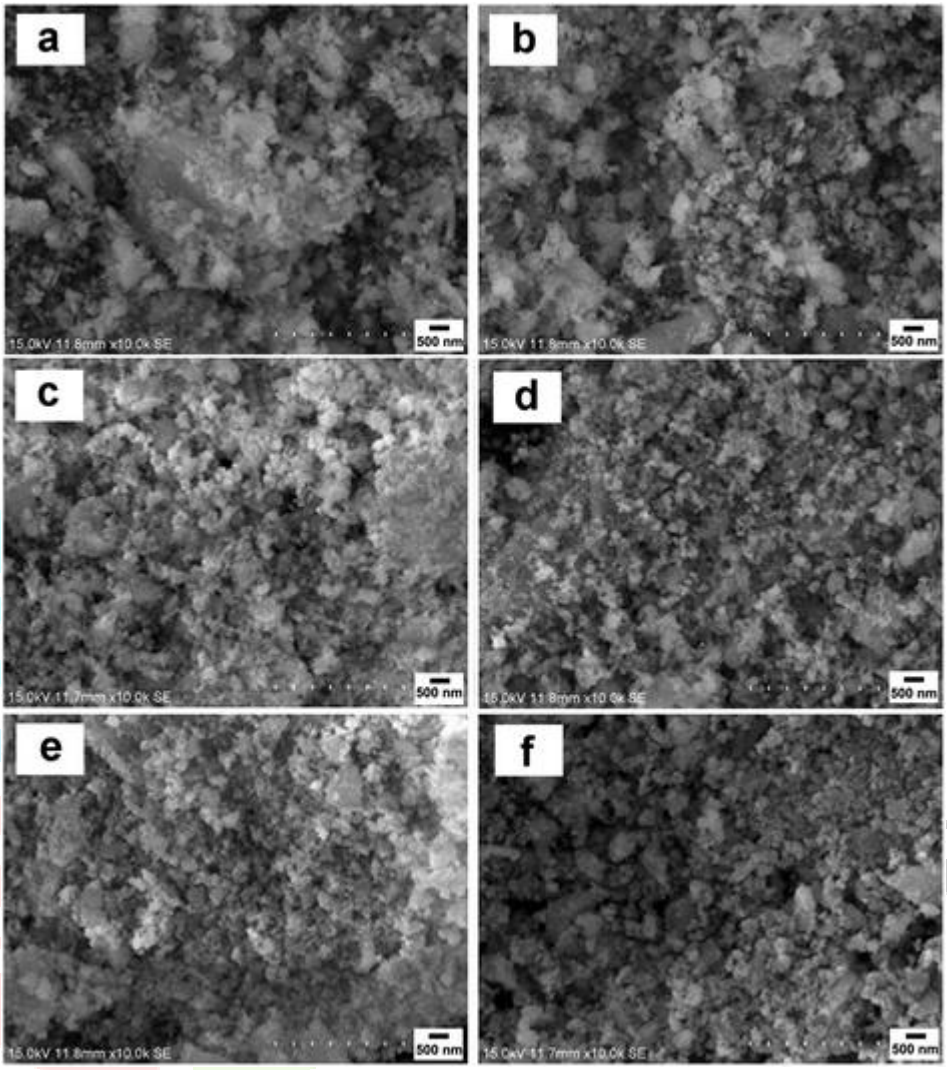

Fig. 3

SEM images of Si-Sb-$(ZnO)_x$ composite materials with different x: 0 (a), 0.1 (b), 0.3 (c), 0.5 (d), 0.7 (e), 0.9 (f)

Figure 4a shows the curves of initial discharge and charge profiles of Si-Sb-$(ZnO)_x$ ($x = 0$, 0.1, 0.3, 0.5, 0.7, 0.9) composite anodes at 0.1 mA/cm^2. The similar trends of all the curves indicate that addition of ZnO hardly affects the mechanism of lithium extraction and insertion for composites. The initial discharge curves are divided into five parts. The first part shows a rapid decrease over 0.8 V, which corresponds to irreversible reaction such as the electrolyte decomposition and the formation of solid electrolyte interface (SEI) film. A discharge plateau appears at about 0.8 V, which is likely due to the reaction of Si-Sb with lithium. The reaction is: $3Li + Si\text{-}Sb \rightarrow Li_3Sb + Si$. The third part of the curve is from 0.8 to 0.5 V, which corresponds to the formation of various Li_xSb compounds. Another discharge plateau appears at about 0.5–0.2 V, which is contributed from the reaction of ZnO with lithium, resulting in the formation of Li_2Zn_5(0.64 V), $LiZn_2$ (0.5 V), Li_2Zn_3 (0.24 V), and LiZn (0.18 V), etc [23]. With the ZnO content increased, this plateau was extended. The fifth part of the curve is below 0.2 V, corresponding to the lithium reaction with Si to form Li_xSi compounds [24, 25]. It is noted that the lithium intercalation potentials for the contents in Si-Sb-$(ZnO)_x$ composite materials are different; they can serve as matrices for each other to

buffer the volume expansion during the lithium intercalation process. Therefore, when Sb reacts with Li at about 0.8 V, Si and ZnO would buffer the volume expansion for Sb; when discharged to about 0.5 V, Si and Sb would alleviate the volume effect of ZnO; Sb and ZnO would inhibit the volume change for Si when the voltage decrease to about 0.2 V. Such processes can improve the electrochemical properties of the composite materials.

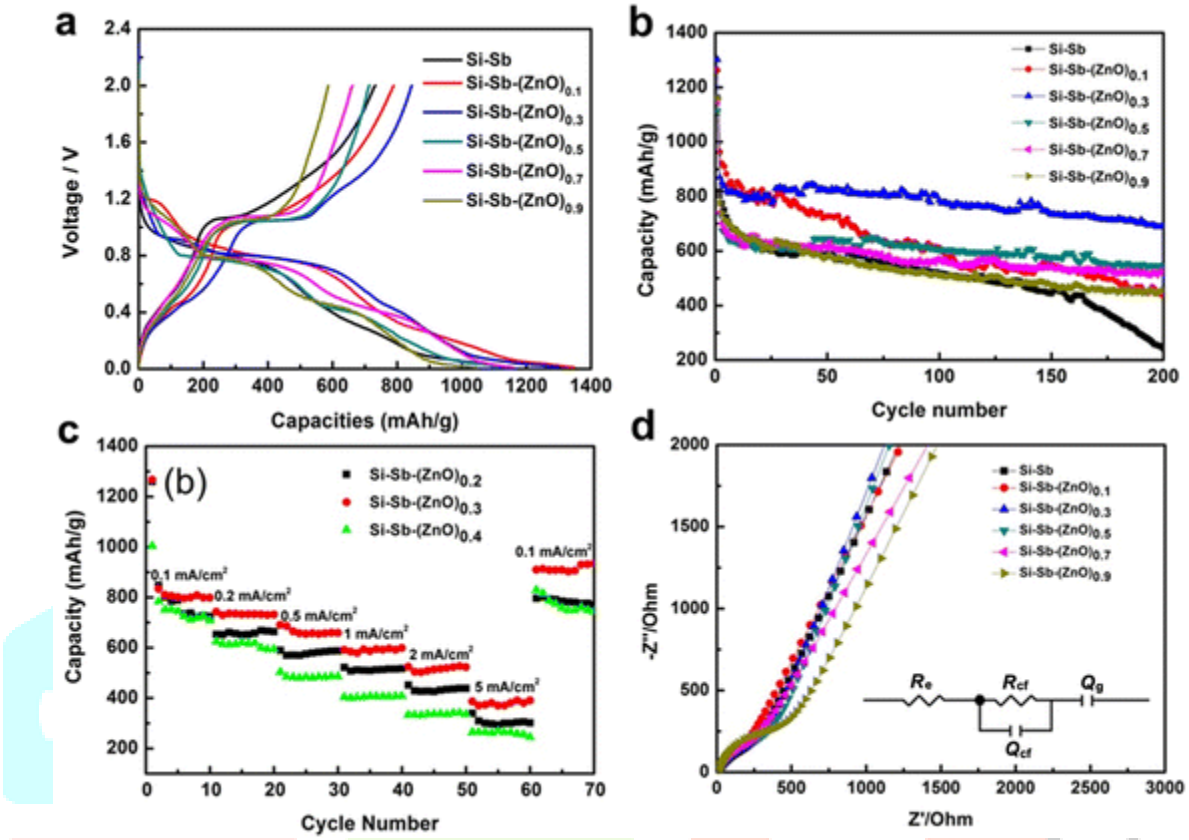

Fig. 4

Voltage profiles (a), cycling performances (b), rate capabilities (c), and electrochemical impedance spectra of Si-Sb and Si-Sb-$(ZnO)_x$composite materials (d). The *inset* of d is the associated equivalent circuit

Cycling performances of Si-Sb-$(ZnO)_x$ composite anode materials were investigated by galvanostatic charge/discharge at 0.1 mA/cm^2; the results are shown in Fig. 4b. The initial discharge capacities of Si-Sb-$(ZnO)_x$ ($x = 0$, 0.1, 0.3, 0.5, 0.7, 0.9) composites are 1161.2, 1262.9, 1301.5, 1159, 1146.9, and 1112.2 mAh/g, respectively. Due to the formation of Sb and Si oxides during the synthesis process which would react with lithium in the first discharge cycle, the irreversible capacities are also increased. The discharge capacities for the second cycle are 818.5, 963, 870.3, 734.4, 740.3, and 777 mAh/g, and the capacities retained at 242.4, 436.8, 690.6, 548.1, 519, and 456.7 mAh/g after 200 cycles. The Si-Sb-$(ZnO)_{0.3}$exhibited 2.5 times of capacity retention compared to Si-Sb alloy and showed the best cycling performance among the composite anode materials. It was demonstrated that with the addition of ZnO, the electrochemical performance of Si-Sb-$(ZnO)_x$ was significantly improved (Additional file 1: Figure S1). The reason is that ZnO has a high theoretical capacity of 978 mAh/g, which could improve the specific capacity of the composite materials. In addition, ZnO was able to effectively relieve the agglomeration of the Si-Sb alloy particles, preventing the loss of electric contact between the current collector and electrode materials induced by volume expansion.

To confirm the superior electrochemical properties of the Si-Sb-$(ZnO)_{0.3}$ composite material, the performance at different current densities was evaluated. As shown in Fig. 4c, the anodes discharged at increasing current densities during the preceding 60 cycles. The initial discharge capacities of Si-Sb-$(ZnO)_x$ ($x = 0.2$, 0.3, 0.4) are 1260, 1267.3 and 1004 mAh/g, respectively, and the average specific capacities decreased as the current density increased. The anode materials became fully lithiated at a low current

density, therefore exhibiting high capacities; while at high current densities, the diffusion of lithium ions in the liquid phase and solid electrode are different, resulting in different equilibrium rates for the reactions, while the capacities decreased. The Si-Sb-$(ZnO)_{0.3}$ composite anode material exhibited the highest discharge capacities among the three composites, even at high current density of 5 mA/cm^2. When the current density varied from 5 to 0.1 mA/cm^2, the discharge capacity of Si-Sb-$(ZnO)_{0.3}$ recovered to 910.8 mAh/g, showing excellent rate capability.

Figure 4d shows the electrochemical impedance of Si-Sb-$(ZnO)_x$ composite anodes and the fitting results before cycling. All the plots were composed of semicircles with a large radius of curvature and sloping lines. The semicircle in the high-frequency intercept represents the contact resistance without lithium insertion, charge transfer, and lithium-ion diffusion at the open voltage [26, 27]. The inset of Fig. 4d shows the impedance responses, which were then analyzed using an equivalent circuit that takes into account all possible contributions to the impedance of the test cell, using R_e as the electrolyte impedance, Q_{cf} and R_{cf}as the contact resistances, and Q_g as the diffusive resistance, and the representative fitting results are shown in Table 2. As can be seen, the appropriate addition of ZnO decreases aggregation in the immiscible Si-Sb system, promoting electrolyte infiltration while reducing the contact resistance of the electrode. However, since the electrical conductivity of ZnO is relatively lower than the alloy, an excess of ZnO addition would lead to the increase of electrode resistance instead.

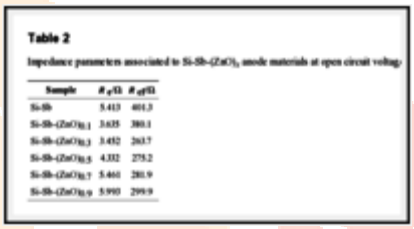

Table 2

Impedance parameters associated to Si-Sb-$(ZnO)_x$ anode materials at open circuit voltage

Cyclic voltammograms of Si-Sb and Si-Sb-$(ZnO)_{0.3}$ composite material were tested in the voltage range of 0–2.0 V (vs. Li/Li$^+$) at a scanning rate of 0.01 mV/s. As shown in Fig. 5, there is almost no change of the curve for the 2nd and 3rd cycles, indicating a high reversibility, and the relatively large difference between the Si-Sb and Si-Sb-$(ZnO)_{0.3}$ is due to the lithium intercalation reactions with ZnO. For the cathodic scan, a low reduction peak is observed in the first cycle at 0.24 V, but disappears in subsequent cycles, corresponding to the reduction of the oxides, the decomposition of the electrolyte, and the formation of SEI film. A strong reduction peak appeared at about 0.8 V and persisted through subsequent cycles, which corresponded to Sb in the Si-Sb alloy reacting with Li to form Li_3Sb. Afterwards, a series of peaks appeared after 0.6 V, corresponding to the reaction of ZnO with Li to form LiZn and the lithiation of Si to form a series of Li_xSi alloys, etc. In the anodic scan, a series of weak peaks appeared at 0.3–0.5 V, corresponding to the de-lithiation of Li_xSi, and the strong peak at 1.1 V was attributed to the formation of Si-Sb alloys.

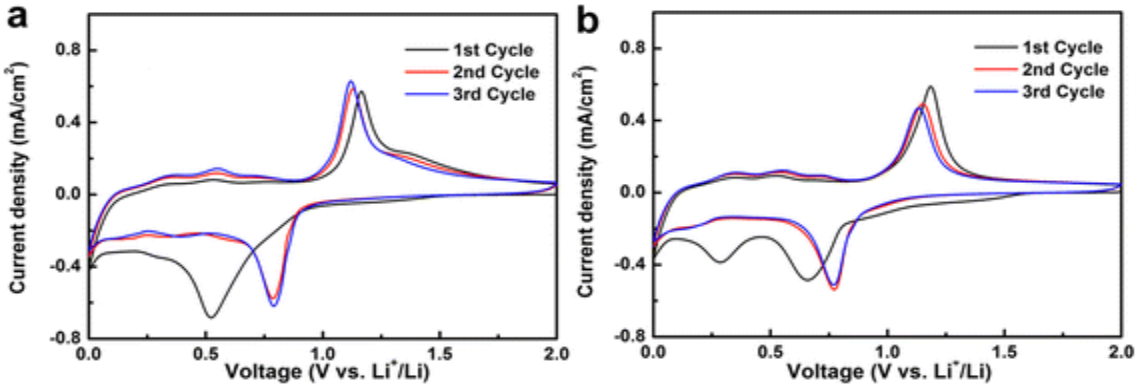

Fig. 5

CV curves of Si-Sb (a), and Si-Sb-$(ZnO)_{0.3}$ (b) composite materials at a scanning rate of 0.01 mV/s

Figure 6 compares the impedance response of Si-Sb-$(ZnO)_x$ and the representative fitting results after the first lithium insertion/extraction cycles. The radius of the semicircles in the low-frequency are observed to increase after the lithium insertion process which is due to the generated Li_xSb, Li_xSi, and Li_xZn packed on the active particles and blocked the transport channels for lithium and electrons, resulting in an increase in the impedance. During de-lithiation process, the composites decomposed, recovering the porous electrode structure and unblocking the channels; therefore, the internal impedance decreased. It is noted that Si-Sb-$(ZnO)_{0.3}$ shows the smallest radius of the semicircle in the low-frequency, indicating the highest electrical conductivity among the composites, which is consistent to the above results.

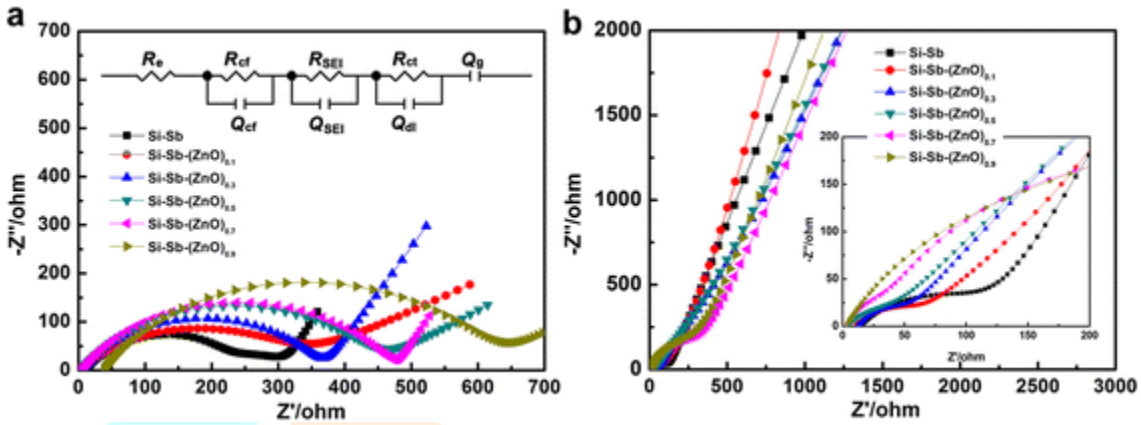

Fig. 6

EIS of Si-Sb-$(ZnO)_x$ anode materials after first lithium insertion (a), and extraction process (b). The inset of a is the associated equivalent circuit

Conclusions

Si-Sb-$(ZnO)_x$ ($x = 0$, 0.1, 0.3, 0.5, 0.7, 0.9) composite anode materials were prepared by a chemical reduction-mechanical alloying method. The materials exhibited superior capacity and good cycling stability for lithium ion-batteries. When the molar ratio of ZnO was 0.3, the initial specific charge capacity and specific discharge capacity of the synthesized Si-Sb-$(ZnO)_{0.3}$ composite anode material were 870.3 and 1301.5 mAh/g, respectively. An appropriate amount of ZnO was able to effectively relieve the agglomeration of the Si-Sb alloy particles, not only greatly shortening the lithium-ion diffusion distance, but also increasing the space available for volume expansions, resulting in greatly improved cycling stability for the Si-Sb-$(ZnO)_x$ composite anode materials. This study gives a rational direction for tailoring the components and structures of composite anode materials to improve the performance of lithium-ion batteries.

References

1. Waag W, Fleischer C, Sauer D. Critical review of the methods for monitoring of lithium-ion batteries in electric and hybrid vehicles. J Power Sources. 2014;258:321–39. doi: 10.1016/j.jpowsour.2014.02.064.

2. Scrosati B, Hassoun J, Sun Y. Lithium-ion batteries. A look into the future. Energy Environ Sci. 2011;4:3287–95. doi: 10.1039/c1ee01388b.

3. Tarascon J, Armand M. Issues and challenges facing rechargeable lithium batteries. Nature. 2001;414:359–67. doi: 10.1038/35104644.

4. Ma D, Cao Z, Hu A. Si-based anode materials for Li-ion batteries: a mini review. Nano-Micro Lett. 2014;6:347–58. doi: 10.1007/s40820-014-0008-2.

5. Liang B, Liu Y, Xu Y. Silicon-based materials as high capacity anodes for next generation lithium ion batteries. J Power Sources. 2014;267:469–90. doi: 10.1016/j.jpowsour.2014.05.096.

6. Yan J, Huang H, Zhang J, Yang Y. The study of Mg_2Si/carbon composites as anode materials for lithium ion batteries. J Power Sources. 2008;175:547–52. doi: 10.1016/j.jpowsour.2007.06.074.

7. Kim H, Choi J, Sohn H, Kang T. The insertion mechanism of lithium into Mg_2Si anode material for Li-ion batteries. J Electrochem Soc. 1999;146:4401–5. doi: 10.1149/1.1392650.

8. Hatchard T, Obrovac M, Dahn J. A comparison of the reactions of the SiSn, SiAg, and SiZn binary systems with Li. J Electrochem Soc. 2006;153:A282–7. doi: 10.1149/1.2140607.

9. Li J, Smith A, Sanderson R, Hatchard T, Dunlap R, Dahn J. In situ $^{\#2}$#1 Mössbauer effect study of the reaction of lithium with Si using a Sn probe. J Electrochem Soc. 2009;156:A283–8. doi: 10.1149/1.3073879.

10. Yu Y, Gu L, Zhu C, Tsukimoto S, Aken P, Maier J. Reversible storage of lithium in silver-coated three-dimensional macroporous silicon. Adv Mater. 2010;22:2247–50. doi: 10.1002/adma.200903755.

11. Lacroix-Orio L, Tillard M, Belin C. Synthesis, crystal and electronic structure of $Li_{13}Ag_5Si_6$, a potential anode for Li-ion batteries. Solid State Sci. 2008;10:5–11. doi: 10.1016/j.solidstatesciences.2007.08.007.

12. Yoon S, Park CM, Kim H, Sohn H. Electrochemical properties of Si-Zn-C composite as an anode material for lithium-ion batteries. J Power Sources. 2007;167:520–3. doi: 10.1016/j.jpowsour.2007.01.096.

13. Hatchard T, Obrovac M, Dahn J. Electrochemical reaction of the $Si_{1-x}Zn_x$ binary system with Li. J Electrochem Soc. 2005;152:A2335–44. doi: 10.1149/1.2098407.

14. Lee H, Lee S. Graphite-FeSi alloy composites as anode materials for rechargeable lithium batteries. J Power Sources. 2002;112:649–54. doi: 10.1016/S0378-7753(02)00461-5.

15. Yu B, Kim H, Park C, Kim S, Sung J, Sohn H. Si Nano-crystallites embedded in Cu-Al-Fe matrix as an anode for Li secondary batteries. Electrochim Acta. 2014;130:583–6. doi: 10.1016/j.electacta.2014.03.067.

16. Wu P, Li J, Tang Y, Xu X, Zhou Y, Chen Y, Lu T. Three-dimensional mesoporous Sn-Ni@C network derived from cyanogel coordination polymers: towards high-performance anodes for lithium storage. Cryst Eng Comm. 2013;15:10340–5. doi: 10.1039/c3ce41647j.

17. Jia H, Stock C, Kloepsch R, He X, Badillo J, Fromm O, Votmann B, Winter M, Placke T. Facile synthesis and lithium storage properties of a porous $NiSi_2$/Si/Carbon composite anode material for lithium-ion batteries. ACS Appl Mater Interf. 2015;7:1508–15. doi: 10.1021/am506486w.

18. Wang J, Wang Y, Zhang P, Zhang D, Ren X. Preparation and electrochemical properties of binary Si_xSb immiscible alloy for lithium ion batteries. J Alloy Compd. 2014;610:308–14. doi: 10.1016/j.jallcom.2014.05.034.

19. Fan L, Zhang J, Zhu Y, Qian Y. Synthesis of urchin-like Sn-ZnO-C composite and its enhanced electrochemical performance for lithium-ion batteries. J Mater Chem. 2014;59:2006–11.

20. Huang X, Xia X, Yuan Y, Zhou F. Porous ZnO nanosheets grown on copper substrates as anodes for lithium ion batteries. Electrochim Acta. 2011;56:4960–5. doi: 10.1016/j.electacta.2011.03.129.

21. Wang H, Pan Q, Cheng Y, Zhao J, Yin G. Evaluation of ZnO nanorod arrays with dandelion-like morphology as negative electrodes for lithium-ion batteries. Electrochim Acta. 2009;54:2851–5. doi: 10.1016/j.electacta.2008.11.019.

22. Pan Q, Qin L, Liu J, Wang H. Flower-like ZnO-NiO-C films with high reversible capacity and rate capability for lithium-ion batteries. Electrochim Acta. 2010;55:5780–5. doi: 10.1016/j.electacta.2010.05.017.

23. Belliard F, Irvine J. Electrochemical performance of ball-milled ZnO-SnO_2 systems as anodes in lithium-ion battery. J Power Sources. 2001;97:219–22. doi: 10.1016/S0378-7753(01)00544-4.

24. Li H, Huang X, Chen L, Zhou G, Zhang Z, Yu D, Mo Y, Pei N. The crystal structural evolution of nano-Si anode caused by lithium insertion and extraction at room temperature. Solid State Ion. 2000;135:181–91. doi: 10.1016/S0167-2738(00)00362-3.

25. Lu Z, Zhu J, Sim D, Shi W, Tay Y, Ma J, Hng H, Yan Q. In situ growth of Si nanowires on graphene sheets for Li-ion storage. Electrochim Acta. 2012;74:176–81. doi: 10.1016/j.electacta.2012.04.046.

26. Song JY, Lee HH, Wang YY, Wan C. Two-and three-electrode impedance spectroscopy of lithium-ion batteries. J Power Sources. 2002;111:255–67. doi: 10.1016/S0378-7753(02)00310-5.

27. Gaberšček M, Pejovnik S. Time evolution of the impedance response of a passive film: a simple application to the Li/$SOCl_2$ system. J Electrochem Soc. 1999;146:933–40. doi: 10.1149/1.1391702.